# A wireless system with a motorized microdrive for neural recording in freely behaving animals

Taku Hasegawa

# Table of Contents

# ABSTRACT

Recordings from single neurons in freely behaving animals provide insights into the brain functions in the natural state. However, isolating activity of single neurons requires the precise positioning of the recording electrodes. Yet, precisely manipulating electrode positions without hindering natural animal behavior is still challenging. Head-mounted assemblies with movable electrodes, called microdrive, have been utilized but the adjustment of the electrodes interferes with animal behaviors. A motorized microdrive system has been developed to precisely control the recording electrodes, permitting single neuronal recordings with less interference; however, animals must be wired for the electrode control and the neural recording, and these wires sometimes become constraints or problematic under the naturally behaving state.

Here, to further expand the range of experiments that can be performed, I developed a neural recording system that combines the motorized microdrive and a wireless interface board using Bluetooth technology. The bidirectional Bluetooth connection allows experimenters to remotely control the microdrive, isolate single neuronal activity in unrestrained animals, and transmit neural signals to a recording PC with a low error rate. Motor driver circuits were simplified and miniaturized, while permitting the precise control of electrodes with the minimal stepping distance of approximately 1.2 μm. Furthermore, to alleviate a load of the digital wireless transmission, a reversible compression method for neural signals was developed, almost halving the transmitting data. With a total weight of 4.2 g (without a battery), the interference to behaviors of animals were minimal, providing the opportunities to study the neural mechanisms of natural behaviors, such as social interaction and exploration within a large area.

# LIST OF SYMBOLS AND ABBREVIATIONS

| | |
|---|---|
| MUA | multi-unit activity |
| SUA | single unit activity |
| WIF | wireless interface |
| SNR | signal-to-noise ratio |
| PF | parafascicular nucleus of the thalamus |
| DV | dorsoventral |
| $V_{PP}$ | peak-to-peak amplitude |
| $W_H$ | half width of trough |
| s.d. | standard deviation |
| s.e. | standard error |

# Chapter 1

# Introduction

## 1.1 *in vivo* extracellular recordings

Brain functions emerge from activity of individual neurons. Electrophysiological recording is one of a few methods that accomplish the investigation of individual activity of neurons with a high temporal resolution[1,2]. In an extracellular recording, an insulated electrode with small exposure at the tip is inserted into brains. Action potentials from a neuron accompany current flows across the cell membrane and hence small electrical fluctuations in the extracellular space. With the close positioning of the electrode tip to the soma of a neuron, actions potentials from only one neuron, or single unit activity (SUA), can be detected. If the electrode tip is not positioned closely to a soma or the exposure of the tip is large, it may capture neuronal activity from many surrounding neurons, leading to a signal mixed with spikes from multiple neurons, called multi-unit activity (MUA). Although it is possible to sort out SUA of several neurons from MUA with spike-sorting methods[3–5], it is crucial to place electrodes close enough to the firing neurons to obtain the high-amplitude spike traces distinguishable from those of other surrounding neurons.

Thus, the extracellular recording for SUA requires the precise positioning of electrodes close to the neuronal soma, and technical effort to stably record from awake, behaving animals has been employed[6,7]. Indeed, measuring neuronal activity from

unrestrained, behaving animals has provided us significant insight for the brain functions responsible for natural behaviors: such as, cognition of spatial location in the hippocampus[8,9], motor learning in the striatum[10,11], and decision making in the prefrontal cortex[12,13]. In some of these studies, multiple electrodes were chronically fixed on the skull to make recordings from a large brain area[9,11]. In other cases, microdrives, which allows experimenters to adjust the vertical position of the electrode by hand, were used to target subpopulations of neurons or small brain areas[8,10,12,13].

## 1.2 Motorized microdrive

The manually adjustable microdrive systems require capturing behaving animals to change the electrode position for the isolation of SUA. The animal handling could interfere with the behaviors, and often such systems utilize low-impedance microwire electrodes, having relatively large tip diameters and providing stable recordings during active behaviors. However, microwire electrodes tend to capture signals from multiple neurons due to their large tip diameters and sometimes difficult to isolate SUA, contrary to sharp electrodes with small tips capable of being positioned proximal to neuronal somas[14]. A bundle of 4 microwires, called a tetrode electrode, facilitates the spike-sorting procedures of SUA from MUA[15,16]; however, even with such tetrode electrodes, SUA are sometimes difficult to be isolated due to the similar spike traces of different neurons or the overlapped traces of simultaneously spiking neurons[17]. Hence, the microdrive systems with manual adjustments are not feasible for recordings from neurons with small soma or neurons with high firing rates, since SUA tend to be hindered by the activity of surrounding neurons with the microwire electrodes.

To overcome the abovementioned problems, a microdrive system that controls electrodes with miniature brushless DC motors was developed[18]. By utilizing motorized

microdrives, electrodes can be controlled without handling animals[18,19] and the isolation of SUA with high-impedance electrodes became practical. With less disturbance on animal behaviors and the precision control of electrodes, this system has provided a novel approach to study in brain functions: such as, the olfactory discrimination of other conspecifics[20] and the temporally precise vocalization of songbirds[21–24].

## 1.3 Telemetry systems for neural recording

Another approach to record neural signals from naturally behaving animals is to send the data of neuronal activity using wireless transmitters mounted on experimental animals[25–34]. Wires between behaving animals and a recording device could be a restraint on voluntary behaviors or locomotion, especially for small animals. It is impractical to record from tethered animals within an open field or arenas with obstacles. In addition, the wires could twist or become entangled during active behaviors, possibly damaging wires or recording systems. By wirelessly transmitting amplified and filtered neural signals as radio waves, for example, wires between animals and recording devices are not necessary. Free from wire-related problems, the range of experiments has been greatly widened; neural recordings from exploring rats within a large arena[25,26], socially communicating primates[27,28], and flying animals such as bats[29] and dragonfly[34] become possible. Although telemetry systems must be powered by some ways, such as batteries[25–33] or high frequency radio waves[34], they provide an opportunity of studying the neural mechanisms of behaviors in natural states.

However, in the previously reported telemetry systems, the recording electrodes were fixed or movable only by hand. Thus, it has been challenging to record SUA with high quality in the telemetry systems. With the best of my knowledge, there has been no

wireless neural recording device that isolates SUA by remotely controlling the recording electrodes, which requires the fine control of electrodes in addition to the transmission of neural signals.

## 1.4 Development of wireless motorized system

Here, I developed a wireless device with a motorized microdrive to isolate and record SUA from awake, freely-moving animals without the constraints imposed by wires. My recording system consists of three components: 1) a motorized microdrive housing three linear actuators, each of which controls the depth of the attached electrode, 2) a wireless interface (WIF) for receiving electrode-driving commands and sending neural signals, and 3) a battery. The WIF is the key component for the communication between the experimenter's computer and the microdrive implanted on the subject. Through the wireless communication, the experimenter can control the electrodes, adjust parameters for recordings, and receive neural signals which will be stored in the computer.

My wireless device is small and lightweight (4.2 g) enough for rats without affecting their behavior, and can continuously transmit neural signals for 3 hours with a 16.0-g battery, or 1 hour with a 4.0-g battery (Table 1). Three electrodes in the microdrive can be independently advanced or retracted with the minimal stepping distance of approximately 1.2 μm, which is small enough for the isolation of SUA. Neural signals from animals can be transmitted up to 5 m with nearly no loss of information, owing to the Bluetooth transmission technology. Moreover, with a newly developed algorithm, neural signals are reversibly compressed in the WIF before being transmitted; this compression process alleviates a load of the wireless transmission, while the original neural signals can be reconstructed in real time. Using my system, single neurons were

recorded from the parafascicular nucleus (PF) of a rat while another rat was introduced in the same arena, which has been difficult with other wireless or tethered recording systems.

| | |
|---|---|
| Motorized Microdrive | 11 (l) × 5 (w) × 17 (h) mm, 1.1 g |
| Wireless Interface (WIF) | 20 (l) × 16 (w) × 7(h) mm, 3.1 g |
| Neural recording | 3 ch., gain 5000x, bandpass 0.1-3 kHz |
| Wireless transmission | Bluetooth Class II, 5 m |
| Power consumption | 360 mW during recording |
| Recording duration | 1 hr with 4-g battery, 3 hr with 16-g battery |

**Table 1 | Specification of Wireless Recording System**

# Chapter 2

# Electrode Control

## 2.1 Chapter Introduction

One challenge of a wireless system is that all electrical circuits need to be incorporated into a highly compact and lightweight form so that a small animal can carry the device. This includes the driver circuit for the electrode control, sets of signal filters and amplifiers, a wireless transmitter, and the controller of the whole device. I designed a compact wireless interface (WIF) which includes all of the above and can be combined with the miniaturized motorized microdrive previously reported[18,24]. In this chapter, I will describe the simplified driver circuit for the electrode control (Section 2.3 to 2.5) and the construction of the miniaturized custom printed circuit board (Section 2.6).

## 2.2 Motorized microdrive

A miniature, motorized microdrive was designed based on previous studies[18,24] (Fig. 1). Briefly, the microdrive, which houses 3 recording electrodes and a 10-pin female connector (Omnetics, Minneapolis, MN), uses sensorless brushless DC motors to drive the electrodes. The motor is 2.4 mm in diameter and 10.8 mm in length, including a gear

head with a 1:337 reduction ratio (Fig. 1 left; SBL02-06H1 PG02-337; Namiki Precision Jewel Company, LTD., Japan). An electrode carrier travels along the threaded motor shaft as the shaft rotates (125-μm pitch), thereby converting a rotation of a motor to a linear motion of an electrode (Fig. 1 right). Thus, with a single turn of the motor, the motor shaft is turned by 1.068° (360° ÷ 337), leading to a vertical movement of the electrode carrier of 0.371 μm (1.068/360 × 125 μm).

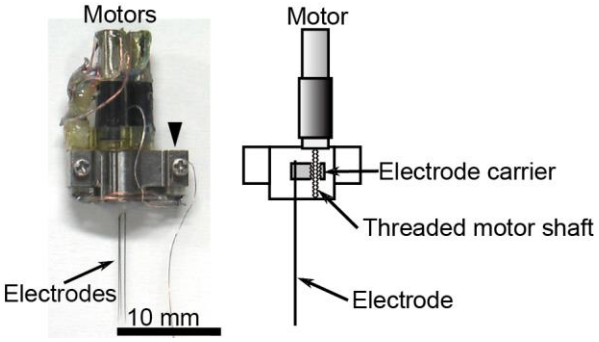


**Fig. 1 | Motorized microdrive.** Left: photograph of a microdrive with 3 motor-electrode pairs. A microdrive is connected to a motor driver and electrophysiological amplifiers through a 10-pin connector (arrowhead). Right: schematic for the linear control of electrode for one motor-electrode pair. Electrode is glued to an electrode carrier, which is attached to a threaded motor shaft.

The microdrive is lightweight (1.1 g) and small (11 × 5 × 17 mm) enough to be mounted on the head of small animals. The motorized microdrive is supplied with motor-driving inputs from a manipulator controller, such as MP-285 (Sutter Instruments; Novato, CA)[18] or a custom printed circuit board[19]. However, the manipulator controllers in the previous studies are too large to be mounted on experimental animals, and therefore a miniaturized driver circuit must be developed.

## 2.3 Simplification of motor-driving signals

A brushless DC motor consists of a permanent magnet as the rotator and coils as the stator (Fig. 2a). By changing the current passing through the coils, a rotating magnetic field is generated and the magnet rotator follows the induced magnetic field. In a

conventional method, three terminals of a motor are supplied with three sinusoidal or square waves with 120◦ phase difference (Fig. 2b). However, with this configuration, a total of nine input lines are required to independently control three motors.

Motor-driving inputs to the microdrive were simplified by modifying the motorized microdrive system previously reported[18]. In the simplified method, two of the three motor terminals are supplied with two square waves with 90◦ phase difference (terminal A and B in Fig. 2c left), while the remaining terminal is supplied with a constant voltage (terminal C in Fig. 2c left); this method still generates a rotating magnetic field (Fig. 2c left). If a constant holding voltage is used instead of one of the two square waves, the magnetic field does not rotate (Fig. 2c right). Since the two input voltages are the same between target and non-target motors (terminal B and C in Fig. 2c), the two input lines are shared with all three motors, while the remaining input line (terminal A in Fig. 2c) is unique to each motor, resulting in a total of 5 lines for driving 3 motors (Fig. 2d).

With this wiring configuration, only a target motor receives two square waves and rotates, while non-target motors are supplied with a holding potential to prevent them from the rotation (Fig. 2e). The travel distance of the electrode in a single move is controlled by changing the number of square pulses (N in Fig. 2e). The direction of the move can be reversed by opposing the phase difference of the two square waves. This simple design allows the miniaturization of the motor driver circuit built into the WIF as shown in the next section.

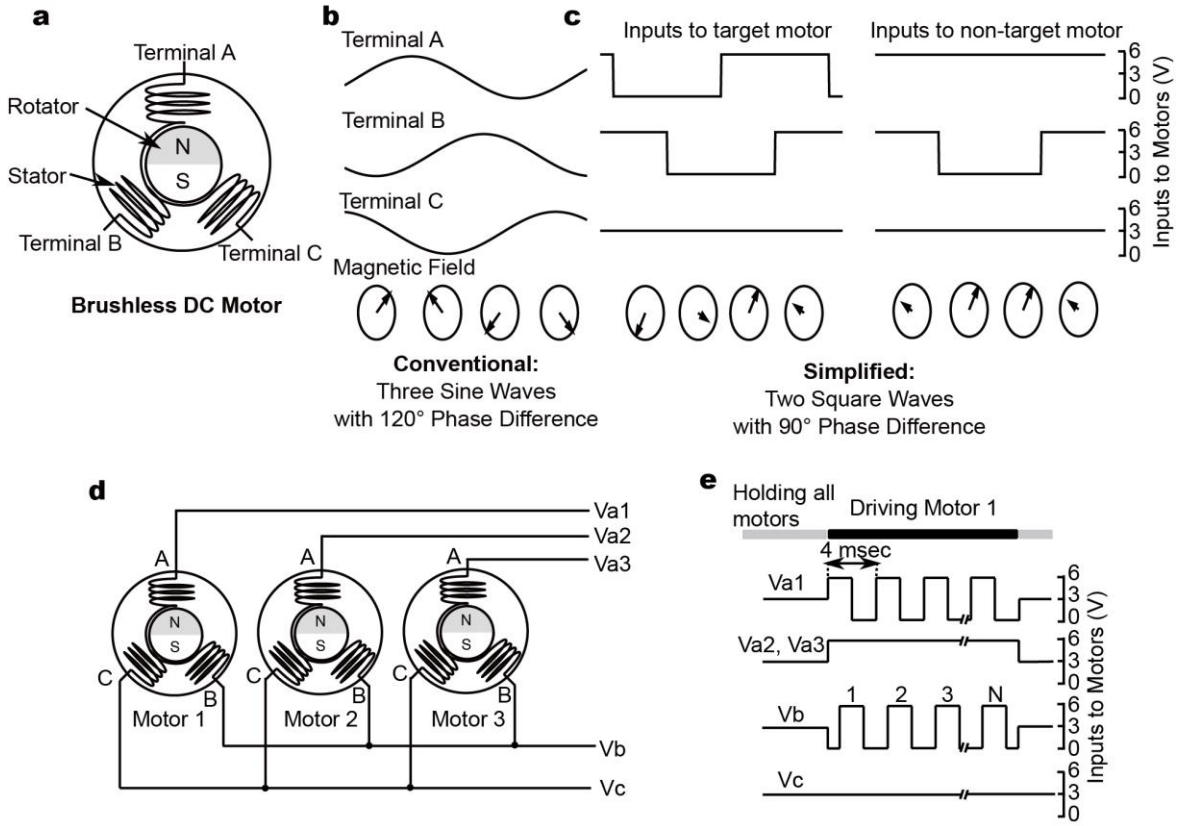


**Fig. 2 | Simplified driving signals for brushless DC motors. a)** Schematic of a brushless DC motor. The rotator is a permanent magnet and the stator is a set of coils. By appropriately changing input voltages to the three terminals (denoted by A, B, and C), the coils generate a rotating magnetic field which turns the rotator magnet. **bc)** Top three: input voltages to each terminal of a DC brushless motor. Bottom: vectors indicating the amplitudes and the direction of the induced magnetic field at different time points during a cycle**. b)** Conventional driving signal. Supplied with three sine waves with 120◦ phase difference, the coils generate a smooth rotating magnetic field. **c)** Simplified motor-driving inputs used in my wireless system. Left: two square waves with 90◦ phase difference, generating a rotating magnetic field. Note that the amplitudes of the vectors are not constant during the cycle. Right: the magnetic field does not rotate, if terminal A is supplied with a holding potential (6 V) instead of the square wave. **d)** Wiring scheme of the motors. Two input lines are shared with all motors so that each motor is supplied with an independent input (Va1, Va2 or Va3) and the two shared inputs (Vb and Vc). **e)** Example of motor-driving signals to drive motor 1. Terminal A of the target motor (Va1) and to terminal B's of all motors (Vb) are supplied with two trains of square pulses with 90°phase difference, while terminal A's of the non-target motors are supplied with a holding potential (Va2, Va3).

## 2.4 Motor driver circuits

To generate square waves in a temporally precise manner, outputs of three analog switches, each supplied with either 0, 3, or 6 V, are short-circuited (Fig. 3). One of the three is turned on from the digital output ports of a microcontroller to output a corresponding voltage at a specific timing (Fig. 3). Since the timings of the digital outputs can be controlled in the order of microseconds, a desired number of square pulses with specific widths and phases can be easily generated.

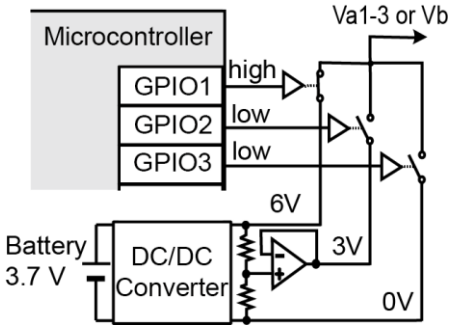


**Fig. 3 | Circuits for generating motor-driving signals.** A DC/DC converter up-converts 3.7 V from a battery to 6 V and an operational amplifier provides 3 V by dividing the converter output. Each of three analog switches is provided with either 0, 3, or 6 V and controlled with general purpose input/output (GPIO) of the microcontroller. The outputs of three analog switches are short-circuited. By turning on one of the switches at a time, a desired number of square pulses with a specific duration and phase can be generated.

In the wiring configuration described in Section 2.2, three input lines unique to each motor (terminal A in Fig. 2c-e), one shared input for square pulses (terminal B in Fig. 2c-e) and one input of a constant voltage (terminal C in Fig. 2c-e) are all the necessary input lines to drive three motors. Four of these 5 input lines, except for the input of a constant voltage, need to be controlled to generate square pulses or a holding potential. Three analog switches are required for each of 4 power lines, and thus a total of 12 analog switches are necessary. I chose to use MAX4602EAE (Maxim Integrated

Products, Sunnyvale, CA, U.S.), which houses 4 analog switches and can provide enough current for driving the brushless DC motors. With 3 of this silicon chip, a total of 12 analog switches were used to design the motor driver circuits.

## 2.5 Precision and linearity of electrode control

My simplified motor driver is of an open-loop control; that is, it does not detect the angular position or rotation of the rotator magnet but only generates motor driving signals. Hence, the displacement of electrodes is not monitored. To characterize the electrode control, the travel distances of the electrodes in response to various pulse numbers were measured.

A microdrive was connected to the driver circuits described in Section 2.4 and the tip of electrode was observed under an inverted microscope (Olympus IX73; 20x objective lens). A motor-driving command for a specific pulse number was sent to the driver circuits. A total displacement of the electrode tip was measured after sending the 10 same motor commands, and the mean displacement per command was calculated (Fig.4).

With less than 5 pulses, the displacement of electrode was small but non-linearly increased as a function of the pulse number. With 5 or more pulses per command, the

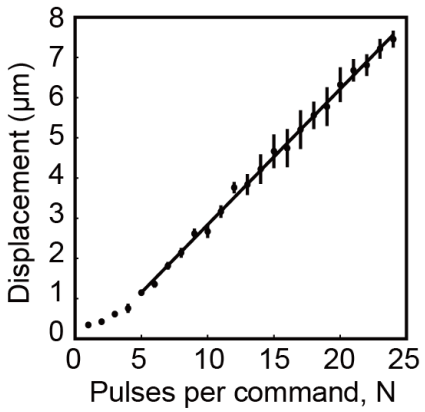


**Fig. 4 | Electrode displacement as a function of pulse number.** Plot showing that the displacement of an electrode is a linear function of a number of pulses within 5 to 24 pulses (displacement (μm) = 0.338N-0.54 for N≥5 with $R^2$=0.997). Vertical line indicates s.e.m.; n=10.

mean displacement per command linearly increased as a function of the number of pulses (Fig. 4; displacement = 0.338 N - 0.54 with $R^2$ = 0.997 for N≥5 where N is the number of pulses).

The non-linearity of electrode movement could be cause by several factors. Since the initial angle of the rotator magnet is not detectable, the first few pulses might not be effective to drive the motor. Alternatively, the static friction within the microdrive requires a larger torque at the initiation of the movement, which possibly leads to the small displacements with driving pulses fewer than 5. Although the cause of the non-linearity is uncertain, the movement is linear and reliable if the motor is supplied with 5 or more pulses. Therefore, a motor driving command with more than or equal to 5 pulses was used; this results in the minimal stepping distance of approximately 1.2 μm, which is small enough to isolate SUA[35].

## 2.6 Design of Wireless Interface board

With the motor driver circuits described above, electrical circuits necessary for wireless neural recording was designed (Fig. 5a). A motorized microdrive is connected to the controller of the wireless system, named as the wireless interface (WIF), which sends motor driving signal, receives and processes neural signal, and wirelessly communicates with an experimenter's computer (Fig. 5a). The system is driven with either a single lithium-polymer battery (Turnigy nano-tech; 3.7 V, 160 mAh, 4.0 g, 39 × 12 × 8 mm) or 4 batteries connected in parallel.

The WIF consists of a custom printed circuit board (Fig. 5b) and a commercially available Bluetooth transceiver (ZEAL-C02; ADC technologies, Nagoya, Japan). A microcontroller (LPC2368; NXP semiconductor, San Jose, CA, U.S.) was used to

process neural signals and to control motor-driving signals through analog switches. The custom printed circuit board was minimized and manufactured by Kanasai Electronics Inc. (Hyogo, Japan), to the extent that the whole system including the motorized microdrive can be mounted on the head of rat (Fig. 5cd).

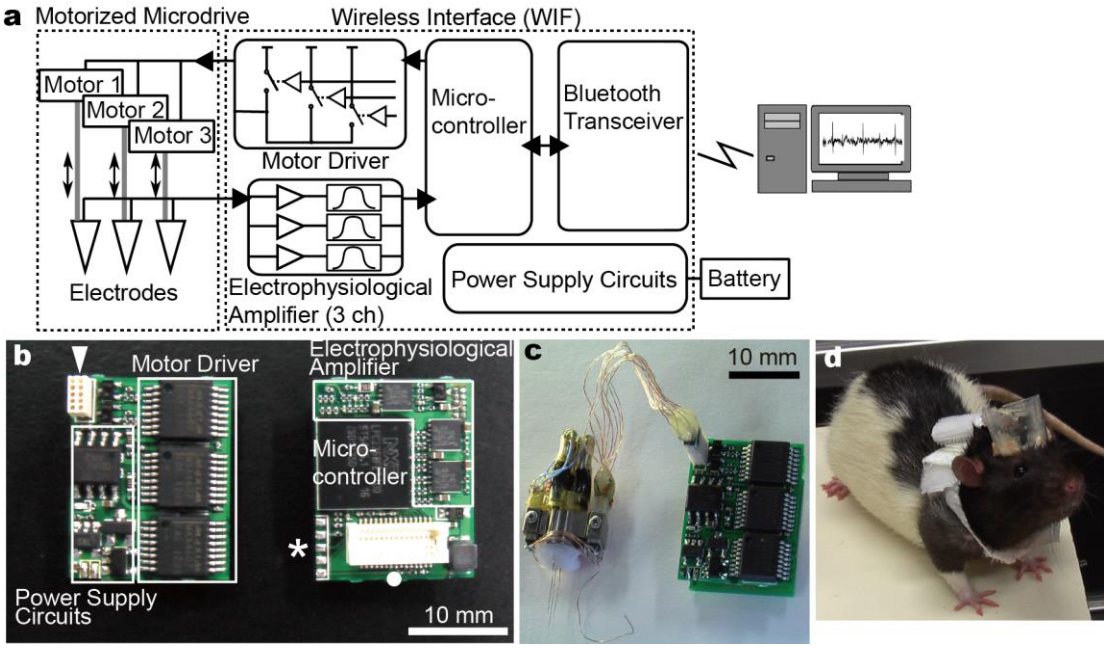


**Figure 5 | A compact wireless interface (WIF) for electrode control, neural signal recording, and wireless data transmission. a)** Schematic for the overall wireless system, consisting of a motorized microdrive, the WIF and a battery. With a command for the electrode control from a computer, the WIF drives a motor in the microdrive, leading to a vertical movement of the recording electrode. Neural signals recorded with the electrode are sent to the WIF where the signals are amplified, bandpass filtered, digitized, and wirelessly sent back to a computer. **b)** Photograph of a custom printed circuit (both sides), consisting of on-board circuits, a microcontroller, the connector for a microdrive (arrowhead) and that for a Bluetooth transceiver (●). The firmware written in the microcontroller may be upgraded through the bare terminals (*). **c)** Photograph of the whole wireless system with the microdrive and the WIF (the custom circuit board in **b** and a Bluetooth transceiver) connected with fine wires. **d)** Photograph of a rat implanted with the microdrive and WIF on the head and equipped with a battery on the back.

## 2.7 Discussion

A previously reported motorized microdrive system uses sinusoidal waves to control the electrodes[18]. The rotation of magnetic field is smooth with sinusoidal waves, but the driver circuits with a flexible control of sinusoidal waves become complicated. By using square pulses instead of sinusoidal ones and by sharing the input lines among motors (Fig. 2de), the driver circuits were greatly simplified to the extent only 12 analog switches, a DC/DC converter, an operational amplifier, and a microcontroller are enough to drive electrodes (Fig. 3). Although the rotation of the magnetic fields is not uniform or smooth and the motor control is open-loop, this newly designed driver circuit showed a robust and precise control of electrodes (Fig. 4). With supplying more than or equal to 5 pulses at a time, the minimal stepping distance of 1.2 μm were achieved, presumably small enough for the isolation of SUA.

As described in section 2.1, a full turn of the rotator in the motor moves the electrode by 0.371 μm to the vertical direction. Since a single square pulse generates a 360◦ rotation of magnetic field, an electrode would move by 0.371 μm per square pulse if the rotator perfectly followed the magnetic field. However, the direct measurements of electrode position resulted in a linear equation: displacement = 0.338 N - 0.54 (N is the pulse number; Fig. 4); that is, the average displacement of electrode per square pulse was estimated to be 0.338 μm with a large pulse number (Fig. 4). This discrepancy is presumably due to the slippage of the rotator in relation to the rotating magnetic field; that is, the rotator fails to follow the rotating magnetic field approximately once in 11 square pulses (0.338/0.371 ≅ 10/11). This is inevitable in the open-loop control of brushless DC motors. With the closed-loop control, the angle of the magnetic rotator is detected and the phase of input voltages can be adjusted. With the feedback control, the

rotation of motor can be controlled without slippage. However, the detection of the rotator angle and the feedback system add another complication to the driver circuits, and they are not implemented in the current system at this point. Further sophistication in the driver circuits can be achieved by introducing the feedback control of the motors.

Based on the simplified motor driver circuits, the controller circuits were manufactured as small as possible to the extent that the WIF along with the motorized microdrive can be mounted on the head of a rat. The key for the miniaturization was to design electrical circuits with a minimal set of electrical parts and to choose small packages of the electrical parts with specifications sufficient for the purpose. Especially, electrical parts that handle large currents such as analog switches should be chosen with care, so that they provide enough current for driving motors while being able to dissipate heat. Similarly, the choice of a microcontroller is crucial; a microcontroller should have enough flash memory, SRAM, processor speed, and peripherals modules such as analog-to-digital converters, although its power consumption and physical size should be minimal.

# Chapter 3

# Wireless Signal Transmission

## 3.1 Chapter Introduction

In a wireless communication system, a sequence of data is transmitted in either analog or digital form. Most analog transmissions use radio waves, and the signal amplitudes are encoded in either the amplitude or frequency modulation. In a digital transmission, signals are encoded in a chunk of binary bits. Analog transmission has advantages in both power consumption and channel capacity; however, the design of an analog circuit is difficult to modify. On the other hand, digital transmissions are more tolerant to noise and are able to be customized. Since the recent developments in digital telecommunication technology have significantly improved energy consumption and

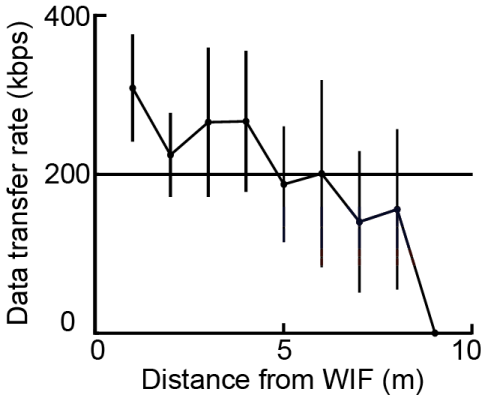


**Fig. 6 | Decreased rates of data transmission across far distances.** The rate may become lower than the minimal requirement of 200 kbps (a horizontal black line with a 20 kHz sampling rate and 10-bit resolution). Mean ± s.d., n=200.

transfer rate, it has become practical to use a digital wireless transmission system for electrophysiological experiments. Therefore, we chose a digital wireless system to transmit neural signals as well as to receive the electrode control commands. Neural signals are A/D converted in a microcontroller and sent to a Bluetooth transceiver, which wirelessly transmits the digitized data to a computer.

During the evaluation of the Bluetooth transceiver, it was observed that the rate of wireless transmission decreases as the distance from the computer increases (Fig. 6). Digitization with a 20 kHz sampling frequency and a 10-bit resolution requires a transmission rate of 200 kbps (20 kHz × 10 bit; horizontal black line in Fig. 6) but the wireless transmission rate could be insufficient under non-ideal circumstances, which leads to a loss of data. To circumvent this problem, amount of data to be transmitted is reduced by developing a reversible compression method.

## 3.2 Theoretical boundary of reversible compression

First, I noticed changes of electrophysiological signals are small in most of time; large deflections of extracellular signals, or action potentials, are of less than 1-msec durations and infrequent (<100 Hz), comprising 10% of recording signals at most. Small changes in signals imply room for data compression. For example, a sequence of alphabets from A to C (such as, “BABCAACB”) can be shortened by one half, by replacing a set of two sequential alphabets with a single alphabet from A to I, following the conversion Table 2 (with this conversion scheme, the above sequence can be expressed as “DFAH”). Intuitively, using only 3 alphabets in this example 3-alphabet sequences contain less information per character, so the sequences can be shortened, or compressed.

| **X** | AA | AB | AC | BA | BB | BC | CA | CB | CC |
|---|---|---|---|---|---|---|---|---|---|
| **Y** | A | B | C | D | E | F | G | H | I |

**Table 2 | Conversion rule from 3-letter ensemble (X) to 9-letter ensemble (Y)**

Claude E. Shannon formally defined amounts of information within a sequence of characters (or values) and showed the theoretical limit for compression efficiency[36]. For an ensemble of characters, $X = \{x_1, x_2, \ldots, x_N\}$, Shannon's information theory defines entropy ($H$) of a sequence as the mean information amount ($I$) per character:

$$I(x_i) \equiv \begin{cases} 0 & \text{if } P(x_i) = 0 \\ -\log_2 P(x_i) & \text{otherwise} \end{cases} \quad (1)$$

$$\mathrm{H}(X) \equiv \sum_{i=1}^{N} P(x_i) I(x_i) \quad (2)$$

where $P(x_i)$ is the probability that character $x_i$ emerges in a sequence. With a base 2 logarithm as shown above, both information amount and entropy have "bit" as a unit. Given a sequence of N data points, any lossless compression methods based on the data distribution cannot covert them to a binary sequence ($Y$) with less than N times the entropy of data, that is:

$$\mathrm{length}(Y) \geq N \times H(X) \quad (3)$$

where length($Y$) is the total bit length, or data size in bits, of compressed data $Y$. Hence the entropy determines the minimum boundary for data size after compression. From eq. (2), note that entropy is determined by a probability of each value in a sequence, or by the distribution of data. Given the same ensemble, the uniform distribution gives the highest entropy and a biased distribution gives low entropy.

Before designing a compression method, the entropy of an electrophysiological signal was calculated (Fig. 7 top). The first-order difference of electrophysiological signal (that is, the change of signal) conveys the same information as the original signal, but its distribution differs from that of the original signals and so entropy does. Considering the possibility of becoming smaller entropy after performing higher-order difference operations, the first-, second-, or third-order differences of the original signal were compared (Fig. 7 from the second to bottom row). Notice that the first-order difference has the narrowest distribution and lowest entropy (4.4 bits). Since the resolution of A/D conversion is 10 bits, the minimum compression ratio achievable with this signal is 44% (a compression ratio is defined as the ratio of the data size of a compressed signal to that of a raw signal; $(4.4 \times N) / (10 \times N) = 0.44$ where N is the number of data points).

For SUA recorded with the WIF in the cortex, hippocampus, and thalamus of anesthetized rats, the first-order difference shows the lowest entropy in every signal (six 60-s signals for each brain area, Fig.8). Therefore, a compression method was constructed with the assumption to take the first-order difference of neural signals.

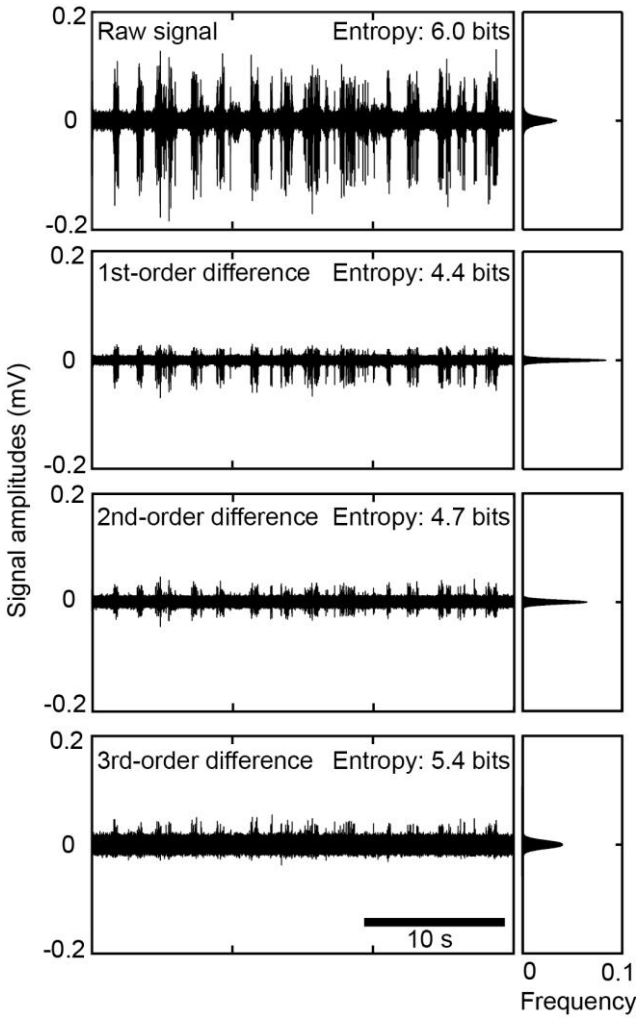


**Fig. 7 | Comparison of the distributions of a raw neural signal and its first-, second-, and third-order differences.** SUA was recorded with the WIF from the cortex of an anesthetized rat with a 20 kHz sampling rate and a 10-bit resolution. Top: raw neural signal (left) and the distribution of each value within the signals (right). Second to Fourth Row: same as top except using the first-, second-, or third-order differences of the same neural signal, respectively. Notice that the first-order difference has the narrowest distribution of amplitude values and the smallest entropy (4.4 bits).

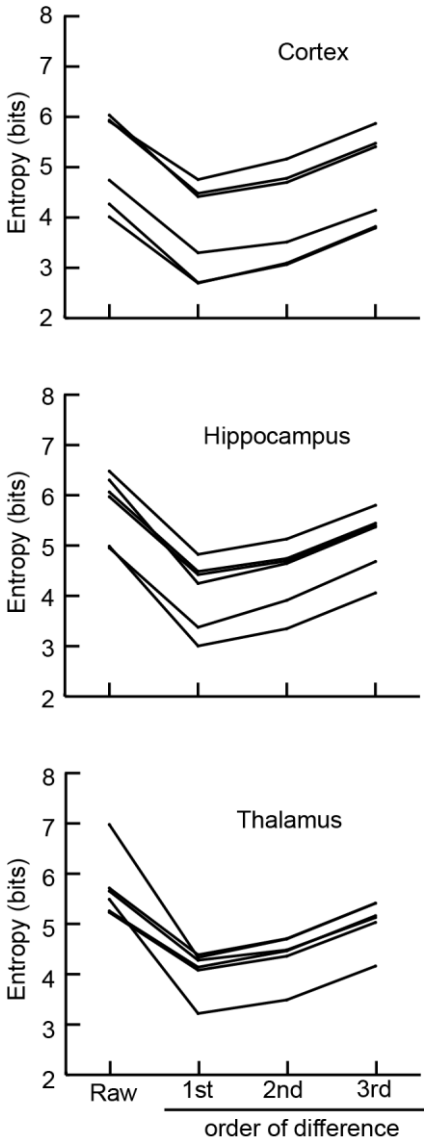


**Fig. 8 | Entropy of raw neural signals or their first-, second- or third-order differences.** SUA from the cortex, hippocampus, and thalamus of anesthetized rats (six 60-s neural signals from each area) were used to assess the theoretical boundary of lossless compression as in Figure 7. Notice that, for every signal, taking the first-order difference results in the smallest entropy.

## 3.3 Realization of data compression

As seen in Section 3.2, the first-order difference of neural signals closely distribute around zero value; that is, higher bits of absolute values of the data tend to be zero and non-informative. Therefore, simply sending only the lower informative bits will reduce the code length without a complicated encoding process. In my coding scheme, a single data point is expressed in three chunks of bits with a fixed compression parameter (k in Fig. 9; k is a positive integer); 1) a sign bit, 2) a unary code that defines the bit length to represent the absolute value of the data, and 3) absolute value of the data (Fig. 9). The compression parameter (k) is the minimum bit length of the informative bits, and should be optimized (discussed in Section 3.4).

Table 3 shows the conversion table for values from -10 to 10 with k=1 to 3. Note that values close to zero is assigned a short code and that the parameter k determines how

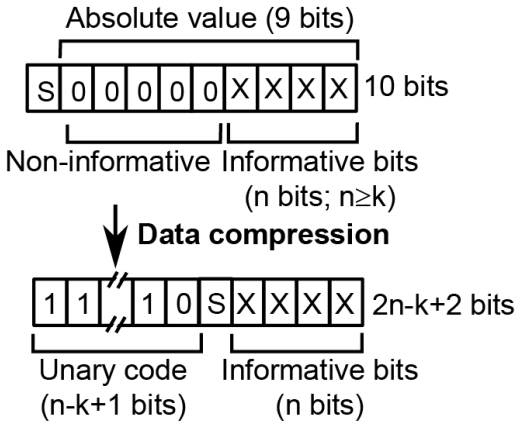


**Fig. 9 | Scheme for data compression.** A single data point is expressed with a sign bit, S, and an absolute value, u. For small absolute values, higher bits of u are mostly 0s and only lower bits are informative; now, an informative bit length, n, is defined as the minimum integer satisfying $2^n > u$ and $n \geq k \geq 0$, where k is a compression parameter. The total bit length after compression is indicated by expressing n – k with a unary code (n - k of successive 1s followed by a single zero). Then, along with the unary code, the sign bit (S) and the informative portion of the absolute value (n bits from the least significant bit) are concatenated.

the code length increases as an input value deviates from zero. For example, with k=0, a value of zero is converted to 2 bits of binary sequence (“00”), shorter than the conversion with k=1 (“000”, 3 bits) or that with k=2 (“0000”, 4 bits). However, as absolute values increase, the length of binary sequences rapidly increases with k=0. The most efficient value for k differs depending on the distribution of data, which is explored in the following section.

This coding method does not require many processor clocks. Figure 10 shows the flow chart of the custom compression method implemented in the microcontroller. The microcontroller can compress a single sample during the idle time between analog-to-digital conversions. The idle time depends on a sampling frequency, but the compression method was confirmed to work with up to a 50 kHz sampling frequency.

| value to be compressed | k=0 | k=1 | k=2 |
|---|---|---|---|
| -10 | 1111011010 | 111011010 | 11011010 |
| -9 | 1111011001 | 111011001 | 11011001 |
| -8 | 1111011000 | 111011000 | 11011000 |
| -7 | 11101111 | 1101111 | 101111 |
| -6 | 11101110 | 1101110 | 101110 |
| -5 | 11101101 | 1101101 | 101101 |
| -4 | 11101100 | 1101100 | 101100 |
| -3 | 110111 | 10111 | 0111 |
| -2 | 110110 | 10110 | 0110 |
| -1 | 1011 | 011 | 0101 |
| 0 | 00 | 000 | 0000 |
| 1 | 1001 | 001 | 0001 |
| 2 | 110010 | 10010 | 0010 |
| 3 | 110011 | 10011 | 0011 |
| 4 | 11100100 | 1100100 | 100100 |
| 5 | 11100101 | 1100101 | 100101 |
| 6 | 11100110 | 1100110 | 100110 |
| 7 | 11100111 | 1100111 | 100111 |
| 8 | 1111001000 | 111001000 | 11001000 |
| 9 | 1111001001 | 111001001 | 11001001 |
| 10 | 1111001010 | 111001010 | 11001010 |

**Table 3 | Example of data compression**

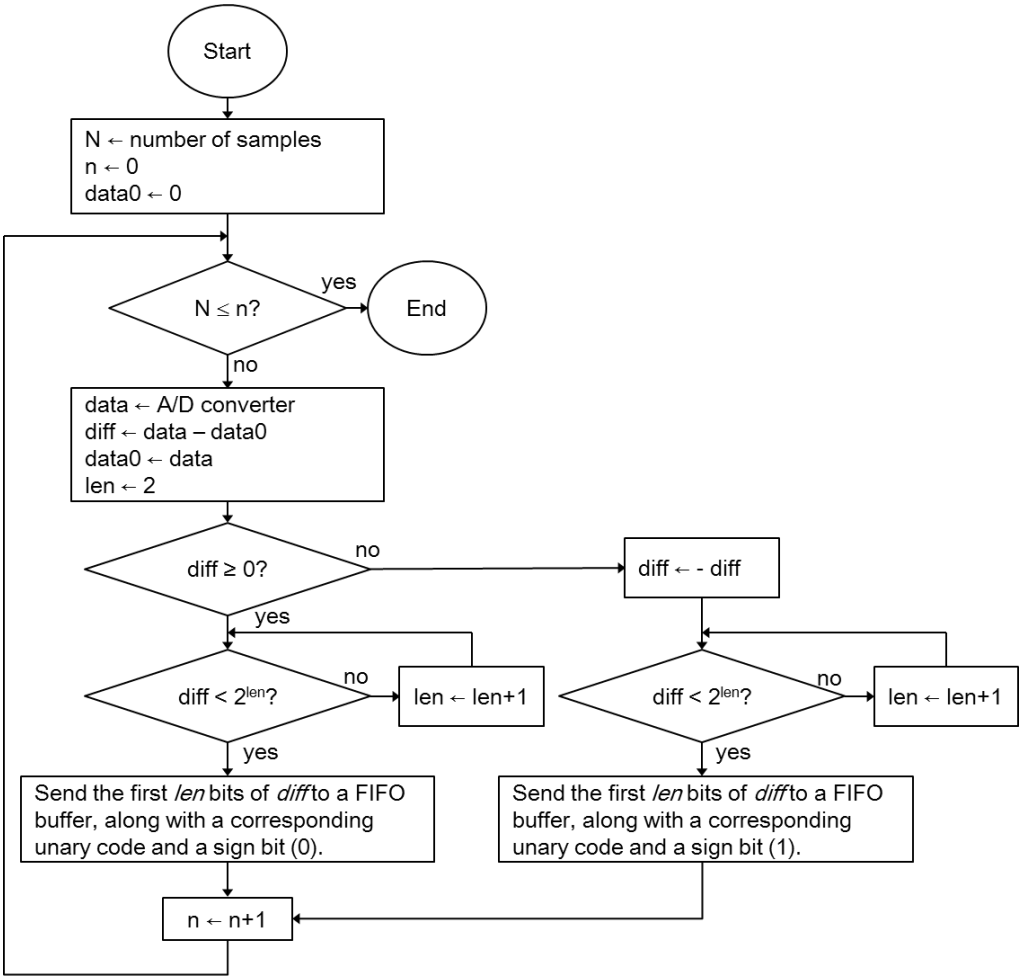


**Fig. 10 | Flow chart for the custom compression method with k=2.** The data compression is performed one sample at a time; that is, during idle time between analog-to-digital conversions (less than 50 μs with a 20-kHz sampling frequency), the microcontroller can compress one sample and store in a FIFO (first-in, first-out) buffer for the wireless transmission. A unary code corresponding to an informative bit length (*len*) is stored as a table in the memory. Explanation for variables: *N*, a total number of samples to be acquired; *n*, a counter for a acquired sample number; *data*, a sample value; *data0*, the sample value from the previous loop; *diff*, the first-order difference of a sample value; *len*, the informative bit length of the absolute value.

## 3.4 Efficiency of data compression

SUA were obtained from the cortex, hippocampus, and thalamus of anesthetized rats, and these neural signals or their first- to third-order differences were compressed with different compression parameters from k=0 to k=5. As expected from the calculation of entropy (Fig. 7 and Fig. 8), the first-order difference resulted in the smallest compressed data size in every data set (Fig. 11). However, the optimal value for parameter k differed from 1 to 3, depending on the neural signals (Fig. 11).

Although the optimal value for k is uncertain before obtaining neural signals, the neural signals are sufficiently small with sub-optimal parameters. With the fixed compression parameter k=2, the compression ratios with the first-order differences were 41.8% to 55.3% (46.7±6.4% for the cortex, 48.4±5.5% for the hippocampus, 47.8±3.2% for the thalamus; mean±s.d.) while the theoretical minimum sizes were 27.0% to 48.4% with the raw signals (37.3±9.4% for the cortex, 40.7±7.1% for the hippocampus, 41.0±4.3% for the thalamus; mean±s.d.) (Fig. 12). Even the fixed compression parameter, the compression scheme was successful and the compression efficiency is approaching to the theoretical limit (Fig. 12). Being close to the theoretical boundary for reversible compression, my encoding method further lowers the requirement of the wireless transmission rate.

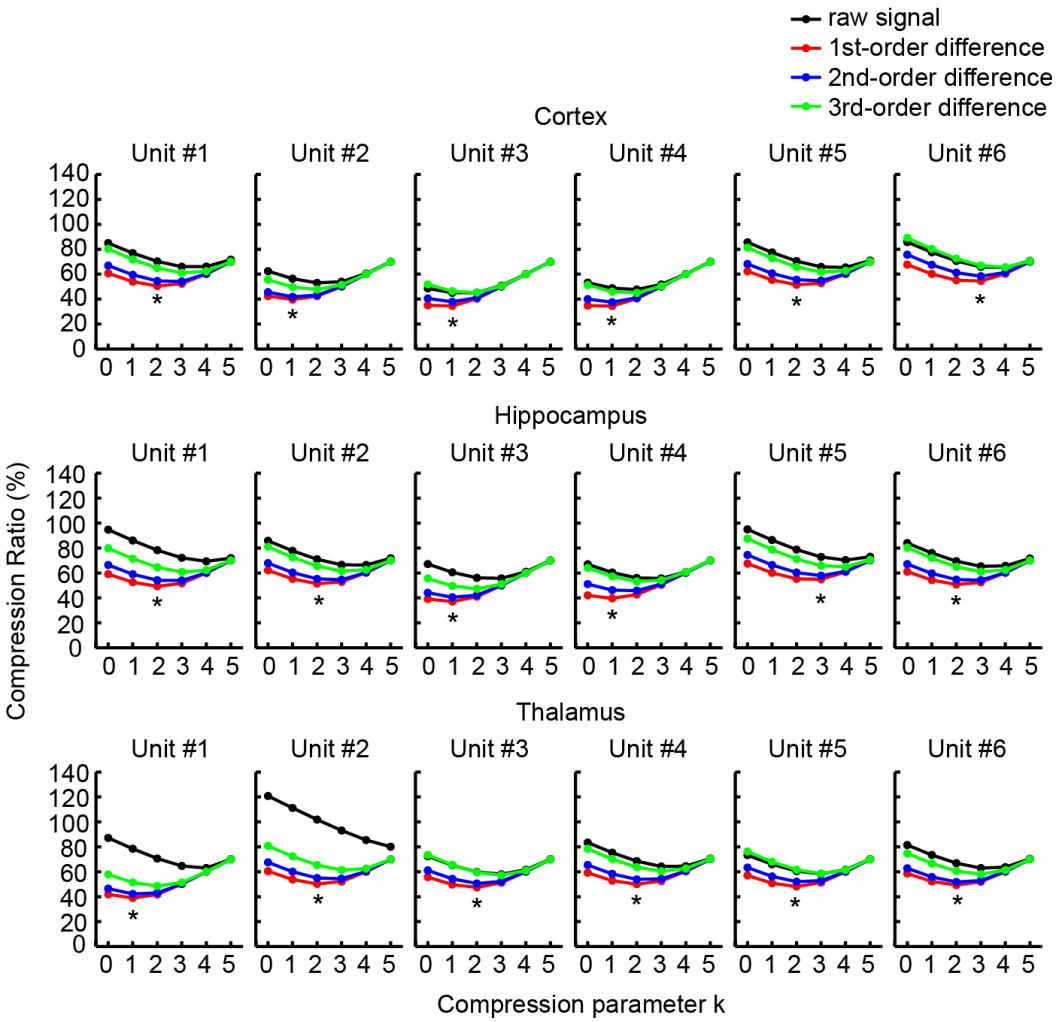


**Fig. 11 | Efficiency of data compression with different pre-processes and compression parameters.** SUA recorded from the cortex, hippocampus, and thalamus of anesthetized rats or their first- to third-order differences were compressed by changing the compression parameter from k=0 to k=5 (60 s, 6 units from each area). Then, the compression ratios were calculated by taking the ratio of the data sizes after compression to the data sizes of the original signals. The smallest data size in each unit signal is indicated with an asterisk. The compression ratios after taking the first-order differences are consistently better than the raw signals or the signals after taking second- or third-order difference. The optimal compression parameter k depends on the characteristics of SUA; 6 units give the smallest data size with k=0, 10 units with k=1, and 2 units with k=0.

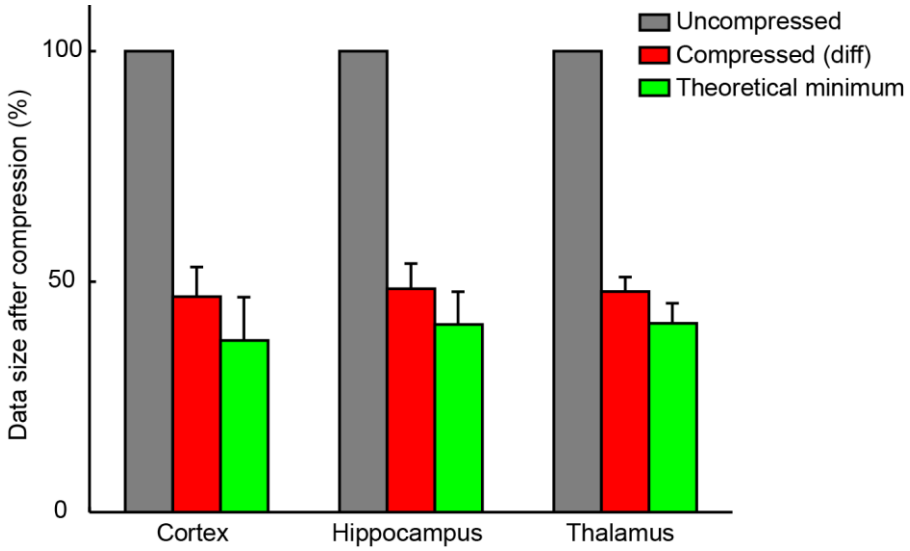


**Fig. 12 | Efficiency of the custom compression method with k=2.** The same data set from Figure 11 was used to examine the compression efficiency of the custom compression method on the first-order differences of neural signals with k=2 (red). The theoretical minimum data sizes were estimated from the entropy of the first-order differences (green). Error bar indicates s.d.; n=6 in each area.

## 3.5 Discussion

Utilizing the properties of electrophysiological signals, my simple compression scheme approximately halves the data size to be transmitted, while the compression can be performed with limited processor resources. Due to its simplicity, the compression process in the microcontroller and the reconstruction of raw neural signals in a computer can be performed in real time, which is crucial for adjusting the electrode positions.

There exists a lossless compression method that achieves the most efficient compression ratio bounded by entropy, called a Huffman code. However, Huffman coding requires extensive calculation both for the generation of a conversion rule and for the conversion itself. Hence, the real-time coding and decoding processes with a

Huffman code would be difficult. With the assumption that the first-order difference of neural signals closely distribute around zero, I constructed a practical, lossless compression method that does not require extensive calculation (Fig. 9 and Fig. 10) and results in only slightly larger data size than the theoretical limit (Fig. 12).Although the optimal compression parameter is either k=1, 2 or 3 depending on the property of the neural signals (Fig. 11), the compression efficiency is sufficiently good with a fixed compression parameter k=2, almost halving the data sizes close to the theoretical limits (Fig. 12). In all of the following experiments, the first-order differences of neural signals were compressed with k=2 before being wirelessly transmitted. With the custom coding scheme, single channel of neural signals can be seamlessly transmitted even under non-ideal circumstances. However, simultaneous recordings from 3 electrodes are still not possible due to the limited transmission rate. Changing the wireless module could overcome this limitation (discussed in Section 5.2).

The parameters for data compression were optimized for my system, by taking the first-order difference of neural signals and by choosing an appropriate value for the compression parameter. The optimization process depends on various factors, such as an amplifier gain, the bandwidth of a bandpass filter, a sampling frequency, and a bit resolution in digitization, as well as the properties of electrophysiological signals. With a higher sampling frequency, a higher-order difference could result in better compression efficiency, and a higher gain would increase the absolute values after digitization as well as an optimal value for the compression parameter. Hence, to utilize this encoding scheme to different digital neural recording systems for the best performance, it is critical to determine the order of difference to take before the compression and the optimal parameter.

# Chapter 4

# Evaluation of Wireless System

## 4.1 Chapter Introduction

The newly developed wireless system was evaluated by recording neuronal activity from anesthetized or awake rats and by performing a behavioral task on rats implanted with the device. First, wirelessly recorded signals were compared to signals simultaneously recorded with a conventional amplifier (Section 4.2). Then, the microdrive and WIF were implanted on a rat and single neuronal activity was isolated from awake, behaving animals (Section 4.3). Finally, the interference of the device implant on animal behaviors was assessed with an operant conditioning task (Section 4.4).

## 4.2 Quality of *in vivo* neural recording

To evaluate the quality of electrophysiological recordings, using the WIF and a conventional recording system, neural signals were simultaneously recorded from the cortex, hippocampus, and thalamus of anesthetized rats. Rats were fixed in a stereotaxic frame, and SUA was isolated with the help of a micromanipulator. In order to simultaneously record neural signals in both the wireless and the wired systems, the

wire between the recording electrode and the WIF was divided and connected to a conventional electrophysiological amplifier (P511; Grass Technologies, West Warwick, RI) with an analog-to-digital converter (PCI-6052E; National Instruments). Then, the two recording systems received the identical signals but process them with different amplifiers, bandpass filters, and digitizers.

A representative neural signal from the thalamus is shown in Figure 13a, demonstrating an extracellular signal from two neurons in the wired and wireless systems. The signal amplitude and the level of background noise were similar between the two systems (Fig. 13a). From traces of all deflections with a negative peak less than -6 μV, a scatter plot with half-trough widths ($W_H$), and peak-to-peak amplitudes ($V_{PP}$) was drawn, showing that the action potentials of two neurons can be clearly differentiated from each other and also distinguished from the background noise (Fig. 13b). The signal-to-noise ratios (SNR) of all action potentials were calculated and averaged for each SUA (Fig. 13c). The mean SNR for all SUA were 22.13 dB and 21.85 dB in the wired and in the wireless systems, respectively. The SNR in the two recording configurations were highly similar between the wired and the wireless systems (Fig. 13c; Pearson's correlation coefficient r=0.9925; n=11).

Although the SNR were comparable between the two systems, spike shapes were slightly different (Fig. 13a right). Although the two systems use bandpass filters with the same bandwidth (0.1 to 3 kHz), it is possible that neuronal spikes were differently attenuated with these bandpass filters, which could result in the difference in spike shapes. Although spike traces are slightly different, neural signals recorded in the wireless system are of comparable quality to those recorded in the wired system.

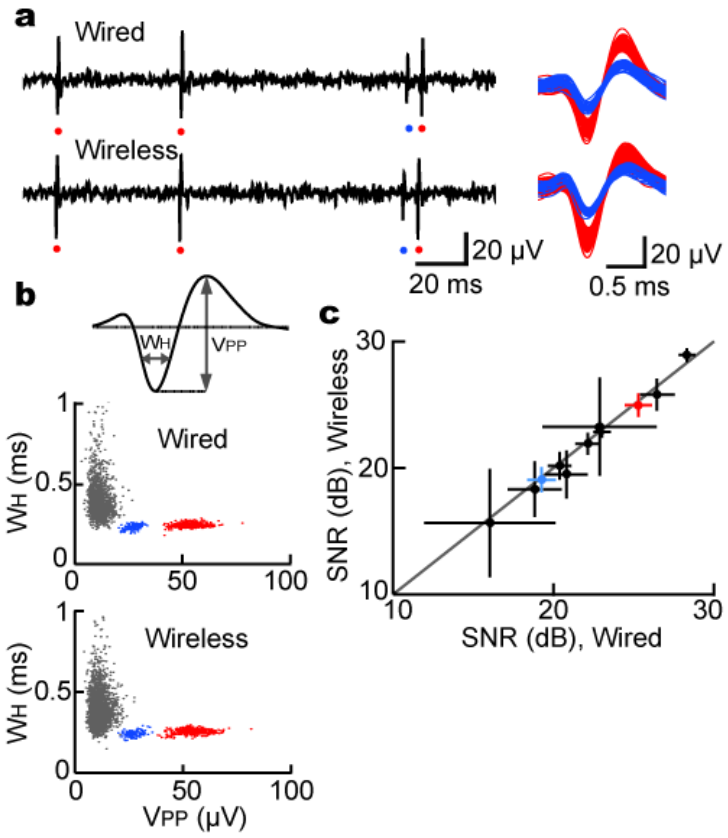


**Fig. 13 | Side-by-side comparison between the wired and wireless systems.** Neural signals are simultaneously recorded in the wired and wireless systems from the cortex, hippocampus, and thalamus of anesthetized rats. **ab)** An example of a neural signal from the thalamus, showing activity of two neurons (red and blue). **a)** Raw signals and spike traces. **b)** A scatter plot to characterize the traces of all deflections with negative peaks below -6 μV, including background noise (grey). The abscissa is the peak-to-peak amplitudes ($V_{PP}$). The ordinate is the widths of the half troughs ($W_H$). **c)** Comparison of signal-to-noise ratios (SNR) between the two systems. Dots and bars indicate means and s.d. of SNR of neural traces, respectively. The SNR are highly similar between the two systems (Pearson's correlation coefficient r=0.9925; n=11).

## 4.3 *in vivo* recording in a freely behaving state

To test if my wireless system is applicable in naturally behaving animals, a microdrive and WIF were implanted on a male rat, targeting one of the thalamic nuclei,

the parafascicular nucleus (PF) (Fig. 14a). After the recovery from the implant surgery, the subject was placed in an 80 cm × 80 cm arena. SUA were isolated during free explorations, and then another rat of the same strain and sex was introduced into the arena (Fig. 14b). By slowly advancing the recording electrode in the order of micrometers, the $V_{PP}$ became larger, presumably reflecting the approach of the electrode tip to the cell body of a spiking neuron (Fig. 14c). In contrast to the increasing amplitude, the $W_H$ of the spike traces did not change during the vertical moves (Fig. 14c); presumably, the recording from the same neuron was maintained during the advance of the electrode, suggesting that the wireless control of electrodes is sufficiently precise to isolate SUA.

The PF is traditionally known as a part of the ascending reticular activating system, and its neurons generate action potentials in response to salient stimuli[37–39]. However, with their direct synaptic connection to striatal cholinergic interneurons[40,41], the PF may also play a role in the selection of motor programs[42–44]. A PF neuron dramatically increased its spiking rate from 11.8 Hz to 34.5 Hz in response to the introduction of another rat (Fig. 14d). The neuron maintained the high firing rate while another rat was present (~5 min), possibly affecting the behavioral bias during the social interaction. Although the increase in the neural activity of PF is consistent with the traditional view for its functions in attention and wakefulness, my wireless system provides the opportunity to study the activity of the PF during social behavior.

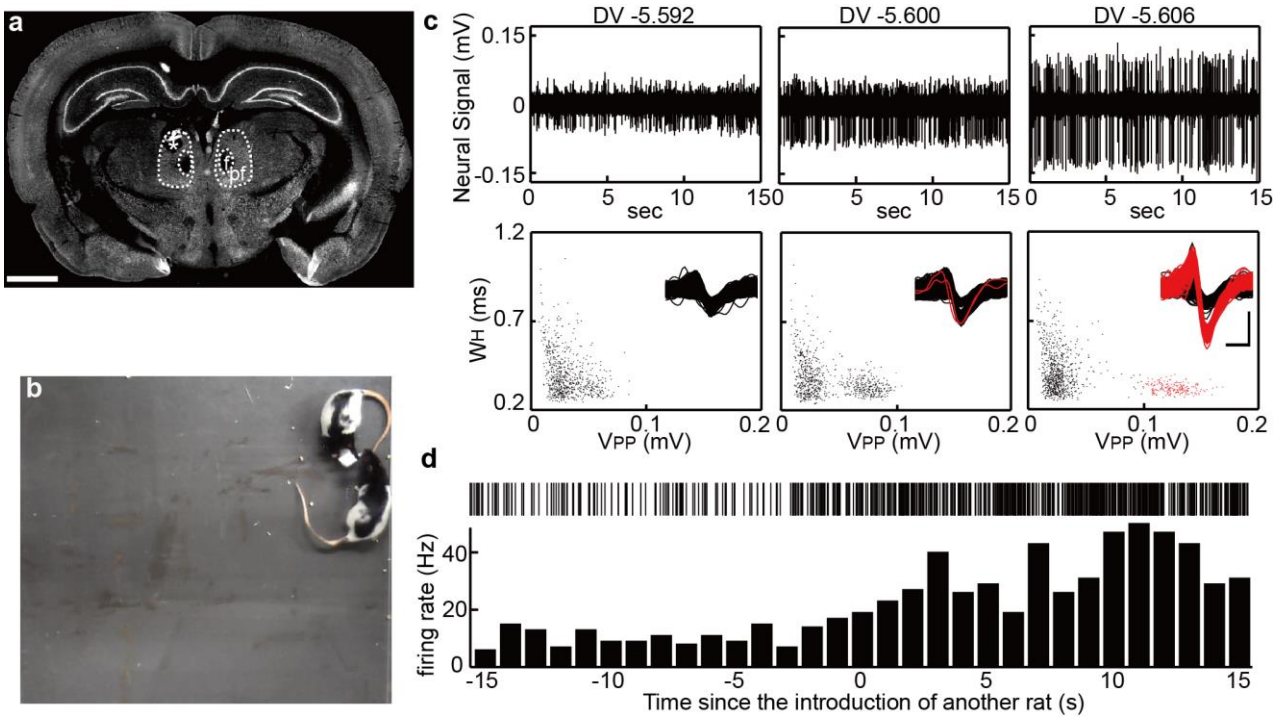


**Fig. 14 | Recordings of SUA during natural behavior. a)** Coronal section immunostained with anti-NeuN antibody, confirming that the recording site (*) was within the parafascicular nucleus (PF) of the left hemisphere. f, fasciculus retroflexus; pf, the parafascicular nucleus (PF); scale bar, 2 mm. **b)** Photograph of a rat socially interacting with another rat. The microdrive and WIF were implanted targeting the PF. **c)** Neural signals (top) and scatter plots (bottom) demonstrating the process of the isolation of SUA from the actively behaving subject. From left to right, the electrode was slowly advanced in the order of micrometers, and SUA of a putative PF neuron was isolated. The dorsoventral (DV) position is indicated on the top of graphs in millimeters. Scatter plots and traces (inset) show all deflections with negative peaks below -20 μV in the neural signals. In the scatter plots, the abscissa is the peak-to-peak amplitudes ($V_{PP}$) and the ordinate is the width of troughs ($W_H$). Deflections with $V_{PP} \geq 0.1$ mV were considered as putative SUA (red dots and traces), while those with $V_{PP} < 0.1$ mV were considered as background noise or activity of surrounding neurons (black dots and traces). Notice that, as the electrode moved down, $V_{PP}$ became larger while $W_H$ did not change, indicating that the same neuron continued to be recorded during the isolation process. Scale bar in inset, 0.5 ms (horizontal) and 100 μV (vertical). **d)** Activity of a putative PF neuron, which changes its firing rate when the rat recognizes another individual. At time 0 s, another rat was introduced to the recording field.

## 4.4 Effect of wireless system on behavior

To test if the implant of wireless systems affects the behavior of animals, rats were trained to perform an operant task and tested their performance before and after the

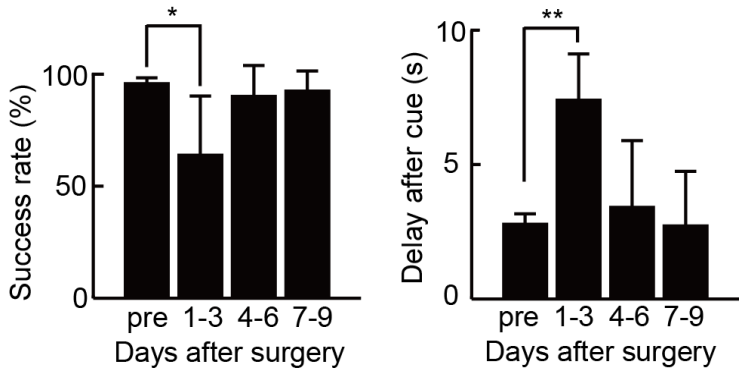


**Fig. 15 | Effect of the wireless recording system on the operant task performance.** The success rates decreased and the responses to the cues were delayed for 3 days after surgery. However, the performance recovered to the pre-surgery level thereafter (n = 5; t-test with pre-surgery). * P < 0.1, ** P<0.05; error bars, s.d.

implant surgery. Rats were water-deprived for 16-18 hr and placed in the operant chamber for a session consisting of 100 trials. In each trial, rats were rewarded with a drop of 10% sucrose water if a lever was pressed after the presentation of a tone cue (1 kHz, 1 s). The trials in which rats pressed the lever within 20 s after the cue presentation were scored as "success". When the success rate reached over 90% for more than 3 consecutive sessions (pre-surgery sessions), the microdrive and WIF were implanted. From the next day of the surgery, 4 batteries (a total of 16.0 g) were mounted on the back of rat, and the effect of the implant surgery was tested in the operant task.

As shown in Figure 15, the mean success rate decreased from 95.7% before surgery to 63.8% in the first 3 days after the surgery (P=0.095; t-test, n=5). Similarly, the delay after cue signal significantly increased from 2.78 ± 0.39 s (mean ± s.d.) before surgery to 7.40 ± 1.72 s (mean ± s.d.) in the first 3 days after the surgery (P=0.013; t-test, n=5). However, the mean success rates and the delay recovered to the pre-surgery level on Day 4-6 and Day 7-9 (P > 0.1).

Since rats recovered to the pre-surgery level within a few days, the initial decline of performance in the operant task is presumably the direct cause of the implant surgery or the anesthesia during the surgery. With recovery time of more than 3 days, rats mounted with the microdrive, the WIF, and the batteries normally performed the operant task, suggesting that interference of the wireless system on the behavior is small.

## 4.5 Discussion

The quality of neuronal signals is one of the most concerns in newly developed recording systems and should be addressed especially in a digital wireless system, in which additional noise sources could be introduced. Radio waves that wirelessly communicate with an experimenter's computer could interfere with neural signals recorded in the electrode; conventionally, Faraday Cage that shields recording systems from incoming electromagnetic or magnetic noises is utilized. Furthermore, switching noise in the digital circuits could be introduced to the amplifier circuits. Indeed, when WIF is directly connected to the recording electrodes, noise with certain frequencies (0.9 kHz, 1.8 kHz, 2.7 kHz, and so on) were observed, presumably caused by digital pulses from the microcontroller or Bluetooth module. Thus, an impedance matching circuit was introduced between the microdrive and WIF, to electrically isolate analog amplifiers from the digital circuits (see Materials and Methods for details). Then, with the impedance matching circuits, the noise level and signal quality in the wireless system were tested and compared with a conventional, wired recording device.

The assessment of the signal quality by simultaneous recordings with a conventional amplifier showed that the signals obtained with the WIF are of comparable quality to the conventional wireless systems, with similar noise levels (Fig. 13a). Although

recorded neural signals are not completely identical, the SNR are highly similar between the two systems (Fig. 13c). No shielding was necessary between the antenna in the Bluetooth transceiver and the recording electrode, even though electromagnetic waves of 2.4 GHz from the Bluetooth transceiver are likely interfere with neural recordings introducing high frequency noise. Presumably, since the noise frequency is almost 1000 times higher than the bandwidth of the bandpass filter (0.1-3 kHz), the high frequency noise was filtered out before the digitization, leaving neural signals unaffected. Also, by closely positioning the impedance matching circuit to the microdrive, noise from digital circuits could be overcome with the electrical isolation of the amplifier circuits from digital circuits.

Neural activity was isolated from a rat socially behaving with another individual (Fig. 14). During active behaviors, the recording electrode was controlled and single neuronal activity was successfully isolated (Fig. 14c). The neural activity gradually became larger as the electrode slowly moved down, thereby isolating SUA from the PF. In addition, the same neuron seemed to be kept recorded during the stepping motions of the electrode, confirming the feasibility of the remote electrode control. Although the success rate of neuronal isolation was not quantified, neuronal signals were stable for more than a few minutes after the isolation, even during active behaviors.

The rat with the microdrive implant normally interacted with another individual. To quantify the effect of device implantation, behaviors of rats were assessed by training an operant conditioning task (Fig. 15). Although the performance became worsened for the first few days after surgery, it recovered to the normal level, suggesting that the microdrive and WIF are lightweight and small enough so that they do not interfere with normal behavioral activity.

# Chapter 5

# Conclusion

## 5.1 Application of the wireless system with motorized microdrive

Previously reported wireless neural recording systems have provided new approaches to study in brain functions of natural behaviors, such as vocal communication in New World monkeys[27,28] or the recognition of three-dimensional space in flying bats[29]. Most of these telemetric systems are designed to transmit as many channels as possible and advantageous when they are combined with multi-channel recording electrodes such as tetrodes, silicon probes, or electrode array.

However, to record SUA in certain brain areas, single sharp electrodes are preferred over multi-channel electrodes. When neurons with small soma are present with a high density or the firing rates of neurons are high, microwire electrodes or silicon probes tend to capture neural activity from multiple neurons. Also, when small brain nuclei are targeted, electrode arrays, which are designed to record from a large brain area, would not be the best choice; silicon probe and tetrodes, having relatively larger diameters, could damage brain tissues, possibly affecting the functions of these nuclei. Therefore,

to complement these previous recording systems, I established a method to wirelessly control electrodes to isolate SUA using a motorized microdrive.

Even with a single electrode, SUA from many neurons could be isolated from an experimental animal by utilizing the motorized microdrive system. By precisely controlling the recording electrodes in the order of micrometers, the electrode tips can be closely positioned to firing neurons, with the help of the real-time monitoring of spike amplitude. Hence, the real-time monitoring is crucial for the isolation and achieved with a newly developed compression method. The compression method alleviates a load of the wireless transmission and allows the transmission of raw electrophysiological signals even with limited processor resources.

My wireless system transforms conventional head-restrained recordings to wireless recordings, which widens the range of experiments that can be performed. Indeed, SUA was isolated and recorded while a rat was freely behaving in an arena with another individual, providing the opportunity for new insights in social interactions. Without using large recording setups or driver circuits but only with a laptop computer, electrophysiological recordings become convenient and applicable to various situations.

## 5.2 Further development of the wireless system

One advantage in my wireless recording system is its high versatility. The motor control and the process of neural signals in the WIF can be modified by updating the firmware of the microcontroller. For example, depending on a brushless DC motor used to control recording electrodes, the motor-driving signals are easily modified by changing the output patterns of the digital I/O ports. Also, instead of using the reversible compression algorithm, an irreversible one could be implemented into the firmware to

increase the number of simultaneous channels to record, as used in other digital wireless systems[32,33]. Taking advantage of the developments in computational and electrical technologies, digital systems can be flexibly adapted to experimental needs.

In my wireless system, the Bluetooth transceiver was chosen from among other digital wireless modules because of the balance between the transfer rate and the battery consumption; in general, the higher the transfer rate, the higher the battery consumption, leading to a shorter recording duration or a heavier battery with high capacity. The transmission of the Bluetooth communication is sufficient for the stable recording from one electrode at a time with the reversible compression. However, to simultaneously record from multiple electrodes, the Bluetooth module can be replaced with wireless LAN module, which consumes higher energy but transmit more data per second by a factor of more than 10. With more simultaneously transmittable channels, silicon probes and tetrodes could be combined with the motorized microdrive.

My wireless system has several limitations including the number of channels to be simultaneously recorded, the level of energy consumption, and also the heavy weight for smaller animals such as mice or songbirds. However, the technique to control electrodes and compress signals can be applied to devices developed in the future. With the ability to wirelessly isolate SUA, this or further improved devices would open new possibilities in neuroscience research.

# MATERIALS AND METHODS

## Animals and surgery

All procedures follow the guideline of the National Institutes of Health and were approved by the Institutional Animal Care and Use Committee of Kyoto University. In the recordings during social interaction and the operant conditioning task, male Long-Evans rats weighing 450-550 g at the time of device implantation were used (Institute for Animal Reproduction, Ibaraki, Japan). In all other experiments, 300-450 g male Wistar rats were used (Japan SLC Inc., Shizuoka, Japan). Animals were reared under a 12:12 hr light:dark cycle with food and water *ad libitum*, except during the operant conditioning in which water was removed 16-18 hr before the experiments.

The motorized microdrive and WIF were anchored on the skull of animal during the anesthesia with an intraperitoneal administration of a ketamine-xylazine mixture (50 mg of ketamine and 2 mg of xylazine per kilogram body weight). After a scalp incision, 10 anchor screws (M1.2 × 2.6; Matsumoto Industry Inc., Chiba, Japan) were drilled into the exposed skull, which was covered with a dual-cure resin cement (BISTITE II, Tokuyama Dental Co., Tokyo, Japan) and an acrylic resin (GC Unifast, GC Corp., Tokyo, Japan). Then, a craniotomy was made above the area of interest and a microdrive was positioned above the area with a stereotaxic manipulator (Narishige Scientific Instrument Lab., Tokyo, Japan). After the smooth insertion of an electrode across the dura was confirmed, the microdrive was fixed on the skull with acrylic resin. Antibiotic-containing ointment was overlaid on the dura to prevent it from drying (Gentacin, MSD K.K., Tokyo, Japan). The WIF was secured with epoxy-based glue to protect it from short circuiting and fixed on the skull next to the microdrive with acrylic

resin. Then, the whole wireless system was secured with a plastic cup. Since batteries need to be replaced for each recording session, they were carried on the back of a rat with a rat jacket (RJ02; Bioresearch center, Nagoya, Japan).

For recordings from the cortex, hippocampus, and thalamus of anesthetized rats, the recording electrodes were positioned -3.5 to -4.0 mm anterior and 2.3 to 2.5 mm lateral from the bregma. For recording from the PF, the microdrive was fixed at -4.0 mm anterior, 1.0 mm lateral from the bregma.

## Histological analysis

After recording sessions, rats were deeply anesthetized with an overdose of sodium pentobarbital (100 mg/kg) and electrolytic lesion was made by passing a DC current (10 μA for 20 s) through recording electrodes as described previously[24], followed by perfusion with phosphate-buffered saline and then 4% formaldehyde in 0.1 M phosphate buffer. Brains were cryoprotected in 30% sucrose and sectioned at 40 μm with a cryostat. The sections were pre-incubated with 10% normal goat serum in PBST (0.01 M phosphate buffered saline containing 0.1% Triton-X-100), incubated with mouse anti-NeuN antibody (1:1000, MAB377; Millipore, Temecula, CA, U.S.) in PBST containing 10% normal goat serum overnight at 4 °C, washed, and then incubated with goat anti-mouse immunoglobulin G conjugated with Alexa 488 (1:500, A11029; Invitrogen, Carlsbad, CA, U.S.) in PBST containing 0.5% normal goat serum for 1 hr at room temperature.

## Data acquisition

In all experiments, tungsten electrodes with 1.2-1.5 MΩ at 1 kHz (WE30031.5B3; MicroProbes for Life Sciences, MD, U.S.) were used. For recordings from behaving

animals, an impedance matching circuit was added to the signal line from the recording electrodes in the microdrive (Fig. 16).

Signals from the electrodes were amplified by 5,000× and bandpass filtered with 0.1-3 kHz. Then, the microcontroller digitized the amplified signals from 0 to 3 V with a 10-bit resolution.

Firmware for the microcontroller, including the custom compression scheme, was written in C. To communicate with the WIF, a desktop or laptop computer (both 64-bit Windows 7) with a USB Bluetooth dongle (BT-MicroEDR2X; Planex Communications Inc., Tokyo, Japan) was used. The neural signals received with the computer were uncompressed by a custom dynamic link library written in C and then analyzed online using a custom LabVIEW program (National Instruments).

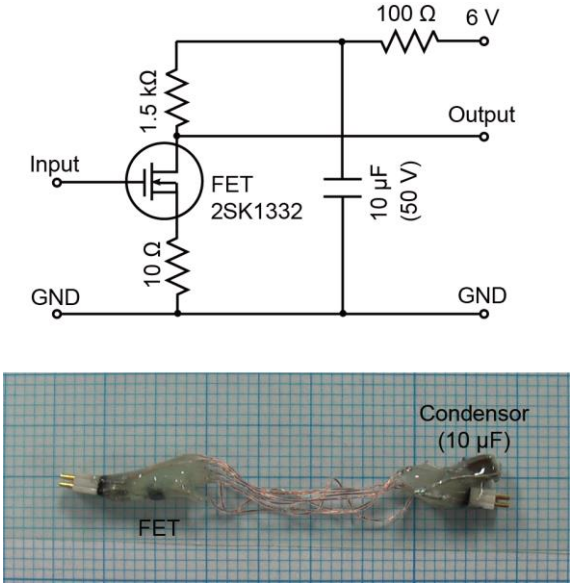


**Figure 16 | Impedance matching circuits for neural signal recording.** Top: circuits for 1 channel of neural signals. Bottom: photograph of the impedance matching circuits, embedded within the wire bundle between the microdrive and WIF. The 10-pin connector with a FET (left) is connected to the microdrive and that with a condenser (right) is connected to the WIF.

## Analysis of neural signals

Offline spike sorting and all statistical analyses were conducted with preinstalled or custom-written MATLAB scripts (Mathworks).

Offline spike sorting was performed in a semi-automated manner based on neural

traces. First, all peaks in the electrophysiological signals exceeding a manually defined threshold were extracted. Then, neural traces around the peaks were analyzed to calculate $V_{PP}$ and $W_H$. $V_{PP}$ was defined as the amplitude difference of the minimum to the maximum value within 1 ms. $W_H$ was defined as the difference in time between the two time points when a voltage crosses the line of the half of amplitude of the peak. Then, $V_{PP}$ and $W_H$ were scatter-plotted and neural spikes were manually clustered. The SNR of isolated spikes were calculated with the equation below, following the previous study[27]:

$$\mathrm{SNR} = 20\ \log_{10}\frac{V_{PP}}{SD_N} \tag{4}$$

where $SD_N$ indicates the standard deviation of the background noise (0.3-0.6 ms preceding all negative peaks).

# REFERENCES


1. Hubel, D. H. & Wiesel, T. N. Receptive fields of single neurones in the cat's striate cortex. *J. Physiol.* **148,** 574–591 (1959).
2. Evarts, E. V. Relation of Discharge Frequency to Conduction Velocity in Pyramidal Tract Neurons. *J. Neurophysiol.* **28,** 216–228 (1965).
3. Lewicki, M. S. A review of methods for spike sorting: the detection and classification of neural action potentials. *Netw. Bristol Engl.* **9,** R53–78 (1998).
4. Quiroga, R. Q., Nadasdy, Z. & Ben-Shaul, Y. Unsupervised Spike Detection and Sorting with Wavelets and Superparamagnetic Clustering. *Neural Comput.* **16,** 1661–1687 (2004).
5. Rutishauser, U., Schuman, E. M. & Mamelak, A. N. Online detection and sorting of extracellularly recorded action potentials in human medial temporal lobe recordings, in vivo. *J. Neurosci. Methods* **154,** 204–224 (2006).
6. Evarts, E. V. A technique for recording activity of subcortical neurons in moving animals. *Electroencephalogr. Clin. Neurophysiol.* **24,** 83–86 (1968).
7. Deadwyler, S. A., Biela, J., Rose, G., West, M. & Lynch, G. A microdrive for use with glass or metal microelectrodes in recording from freely-moving rats. *Electroencephalogr. Clin. Neurophysiol.* **47,** 752–754 (1979).
8. O'Keefe, J. & Dostrovsky, J. The hippocampus as a spatial map. Preliminary evidence from unit activity in the freely-moving rat. *Brain Res.* **34,** 171–175 (1971).
9. Agarwal, G. *et al.* Spatially Distributed Local Fields in the Hippocampus Encode Rat Position. *Science* **344,** 626–630 (2014).
10. Barnes, T. D., Kubota, Y., Hu, D., Jin, D. Z. & Graybiel, A. M. Activity of striatal neurons reflects dynamic encoding and recoding of procedural memories. *Nature* **437,** 1158–1161 (2005).
11. Jin, X. & Costa, R. M. Start/stop signals emerge in nigrostriatal circuits during sequence learning. *Nature* **466,** 457–462 (2010).
12. Kepecs, A., Uchida, N., Zariwala, H. A. & Mainen, Z. F. Neural correlates, computation and behavioural impact of decision confidence. *Nature* **455,** 227–231 (2008).
13. Karlsson, M. P., Tervo, D. G. R. & Karpova, A. Y. Network Resets in Medial Prefrontal Cortex Mark the Onset of Behavioral Uncertainty. *Science* **338,** 135–139 (2012).
14. Hubel, D. H. Tungsten Microelectrode for Recording from Single Units. *Science* **125,**

549–550 (1957).

15. Wilson, M. A. & McNaughton, B. L. Dynamics of the hippocampal ensemble code for space. *Science* **261,** 1055–1058 (1993).
16. O'Keefe, J. & Recce, M. L. Phase relationship between hippocampal place units and the EEG theta rhythm. *Hippocampus* **3,** 317–330 (1993).
17. Harris, K. D., Henze, D. A., Csicsvari, J., Hirase, H. & Buzsáki, G. Accuracy of Tetrode Spike Separation as Determined by Simultaneous Intracellular and Extracellular Measurements. *J. Neurophysiol.* **84,** 401–414 (2000).
18. Fee, M. S. & Leonardo, A. Miniature motorized microdrive and commutator system for chronic neural recording in small animals. *J. Neurosci. Methods* **112,** 83–94 (2001).
19. Yamamoto, J. & Wilson, M. A. Large-scale chronically implantable precision motorized microdrive array for freely behaving animals. *J. Neurophysiol.* **100,** 2430–2440 (2008).
20. Luo, M., Fee, M. S. & Katz, L. C. Encoding pheromonal signals in the accessory olfactory bulb of behaving mice. *Science* **299,** 1196–1201 (2003).
21. Hahnloser, R. H. R., Kozhevnikov, A. A. & Fee, M. S. An ultra-sparse code underliesthe generation of neural sequences in a songbird. *Nature* **419,** 65–70 (2002).
22. Prather, J. F., Peters, S., Nowicki, S. & Mooney, R. Precise auditory–vocal mirroring in neurons for learned vocal communication. *Nature* **451,** 305–310 (2008).
23. Prather, J. F., Nowicki, S., Anderson, R. C., Peters, S. & Mooney, R. Neural correlates of categorical perception in learned vocal communication. *Nat. Neurosci.* **12,** 221–228 (2009).
24. Fujimoto, H., Hasegawa, T. & Watanabe, D. Neural Coding of Syntactic Structure in Learned Vocalizations in the Songbird. *J. Neurosci.* **31,** 10023–10033 (2011).
25. Szuts, T. A. *et al.* A wireless multi-channel neural amplifier for freely moving animals. *Nat. Neurosci.* **14,** 263–269 (2011).
26. Ball, D. *et al.* Rodent Scope: A User-Configurable Digital Wireless Telemetry System for Freely Behaving Animals. *PLoS ONE* **9,** e89949 (2014).
27. Roy, S. & Wang, X. Wireless multi-channel single unit recording in freely moving and vocalizing primates. *J. Neurosci. Methods* **203,** 28–40 (2012).
28. Hage, S. R., Jürgens, U. & Ehret, G. Audio–vocal interaction in the pontine brainstem during self-initiated vocalization in the squirrel monkey. *Eur. J. Neurosci.* **23,** 3297–3308 (2006).
29. Yartsev, M. M. & Ulanovsky, N. Representation of Three-Dimensional Space in the

Hippocampus of Flying Bats. *Science* **340,** 367–372 (2013).

30. Schregardus, D. S. *et al.* A lightweight telemetry system for recording neuronal activity in freely behaving small animals. *J. Neurosci. Methods* **155,** 62–71 (2006).
31. Ruther, P. *et al.* Compact wireless neural recording system for small animals using silicon-based probe arrays. in *2011 Annual International Conference of the IEEE Engineering in Medicine and Biology Society,EMBC* 2284–2287 (2011). doi:10.1109/IEMBS.2011.6090575
32. Hampson, R. E., Collins, V. & Deadwyler, S. A. A wireless recording system that utilizes Bluetooth technology to transmit neural activity in freely moving animals. *J. Neurosci. Methods* **182,** 195–204 (2009).
33. Aceros, J., Yin, M., Borton, D. A., Patterson, W. R. & Nurmikko, A. V. A 32-channel fully implantable wireless neurosensor for simultaneous recording from two cortical regions. in *2011 Annual International Conference of the IEEE Engineering in Medicine and Biology Society,EMBC* 2300–2306 (2011). doi:10.1109/IEMBS.2011.6090579
34. Thomas, S. J., Harrison, R. R., Leonardo, A. & Reynolds, M. S. A battery-free multichannel digital neural/EMG telemetry system for flying insects. *IEEE Trans. Biomed. Circuits Syst.* **6,** 424–436 (2012).
35. Barmack, N. H. & Hayes, D. F. A stepper motor controlled microdrive for recording from unanesthetized animals. *Physiol. Behav.* **5,** 705–706 (1970).
36. MacKay, D. J. C. *Information theory, inference, and learning algorithms*. (Cambridge University Press, 2003).
37. Steriade, M. & Demetrescu, M. Unspecific Systems of Inhibition and Facilitation of Potentials Evoked by Intermittent Light. *J. Neurophysiol.* **23,** 602–617 (1960).
38. Minamimoto, T. & Kimura, M. Participation of the Thalamic CM-Pf Complex in Attentional Orienting. *J. Neurophysiol.* **87,** 3090–3101 (2002).
39. Raeva, S. N. The Role of the Parafascicular Complex (CM-Pf) of the Human Thalamus in the Neuronal Mechanisms of Selective Attention. *Neurosci. Behav. Physiol.* **36,** 287–295 (2006).
40. Ding, J. B., Guzman, J. N., Peterson, J. D., Goldberg, J. A. & Surmeier, D. J. Thalamic Gating of Corticostriatal Signaling by Cholinergic Interneurons. *Neuron* **67,** 294–307 (2010).
41. Threlfell, S. *et al.* Striatal Dopamine Release Is Triggered by Synchronized Activity in Cholinergic Interneurons. *Neuron* **75,** 58–64 (2012).
42. Minamimoto, T., Hori, Y. & Kimura, M. Complementary Process to Response Bias in the Centromedian Nucleus of the Thalamus. *Science* **308,** 1798–1801 (2005).

43. Brown, H. D., Baker, P. M. & Ragozzino, M. E. The Parafascicular Thalamic Nucleus Concomitantly Influences Behavioral Flexibility and Dorsomedial Striatal Acetylcholine Output in Rats. *J. Neurosci.* **30,** 14390–14398 (2010).
44. Minamimoto, T., Hori, Y. & Kimura, M. Roles of the thalamic CM-PF complex-Basal ganglia circuit in externally driven rebias of action. *Brain Res. Bull.* **78,** 75–79 (2009).

# ACKNOWLDEGEMENT

This works is conducted in the Department of Molecular and Systems Biology, Graduate School of Biostudies, Kyoto University. Dr. Dai Watanabe conceived the project. Dr. Hisataka Fujimoto developed the motorized microdrive systems. Mr. Koichiro Tashiro and Dr. Akira Tsuchiya designed the electrical circuits. Ms. Mayu Nonomura helped behavioral experiments. I also thank Dr. Kosuke Hamaguchi for helpful comments.

*This thesis is based on the material contained in the following article.*

Taku Hasegawa, Hisataka Fujimoto, Koichiro Tashiro, Mayu Nonomura, Akira Tsuchiya, and Dai Watanabe.

**A wireless neural recording system with a precision motorized microdrive for freely behaving animals.**

Scientific Reports, **5**, 7853, 19 January 2015.